JOURNAL OF AGRICULTURAL AND FOOD CHEMISTRY

Agricultural and Environmental Chemistry

Synthesis and Docking Study of N-(Cinnamoyl)-N#-(Substituted)acryloyl Hydrazide Derivatives Containing Pyridinium Moieties as a Novel Class of FtsZ Inhibitors against the Intractable Xanthomonas oryzae pv. oryzae Infections in Rice

Xiang Zhou, Yu-Mei Feng, Pu-Ying Qi, Wu-Bin Shao, Zhibing Wu, Li-Wei Liu, Yi Wang, Hao-Dong Ma, Pei-Yi Wang, Zhong Li, and Song Yang

J. Agric. Food Chem., **Just Accepted Manuscript** • DOI: 10.1021/acs.jafc.0c01565 • Publication Date (Web): 10 Jul 2020

is published by the American Chemical Society. 1155 Sixteenth Street N.W., Washington, DC 20036

Synthesis and Docking Study of *N*-(Cinnamoyl)-*N′*-(Substituted)acryloyl Hydrazide Derivatives Containing Pyridinium Moieties as a Novel Class of FtsZ Inhibitors against the Intractable *Xanthomonas oryzae* pv. *oryzae* Infections in Rice

Xiang Zhou [†], Yu-Mei Feng [†], Pu-Ying Qi [†], Wu-Bin Shao [†], Zhi-Bing Wu [†], Li-Wei Liu [†], Yi Wang [†], Hao-Dong Ma [†], Pei-Yi Wang* [†], Zhong Li [‡], Song Yang* [†] [‡]

[†] State Key Laboratory Breeding Base of Green Pesticide and Agricultural Bioengineering, Key Laboratory of Green Pesticide and Agricultural Bioengineering, Ministry of Education, Center for R & D of Fine Chemicals of Guizhou University, Guiyang 550025, China

[‡] College of Pharmacy, East China University of Science & Technology, Shanghai 200237, China

* Corresponding author.

E-mail: jhzx.msm@gmail.com (S. Yang), pywang888@126.com (P.-Y. Wang).

Abstract

Xanthomonas oryzae pv. *oryzae* (*Xoo*) is an offensive phytopathogen that can invade a wide range of plant hosts to develop bacterial diseases, including the well-known rice bacterial leaf blight. However, few agrochemicals have been identified to effectively prevent and eliminate *Xoo*-induced diseases. Thus, designing novel antibacterial compounds on the basis of the potential targets from *Xoo* may lead to the discovery of highly efficient and innovative anti-*Xoo* agents. Filamentous temperature-sensitive protein Z (FtsZ), an important functional protein in the progression of cell division, has been widely reported and exploited as a target for creating antibacterial drugs in the field of medicine. Therefore, the fabrication of innovative frameworks targeting *Xoo*FtsZ may be an effective method for managing bacterial leaf blight diseases via blocking the binary division and reproduction of *Xoo*. As such, a series of novel *N*-(cinnamoyl)-*N*′-(substituted)acryloyl hydrazide derivatives containing pyridinium moieties was designed, and the anti-*Xoo* activity was determined. The bioassay results showed that compound $\mathbf{A_7}$ had excellent anti-*Xoo* activity (EC_{50} = 0.99 mg L^{-1}) in vitro and distinct curative activity (63.2% at 200 mg L^{-1}) in vivo. Further studies revealed that these designed compounds were *Xoo*FtsZ inhibitors, validating by the reduced GTPase activity of recombinant *Xoo*FtsZ, the nonfilamentous *Xoo*FtsZ assembly observed in the TEM images, and the prolonged *Xoo* cells from the fluorescence patterns. Computational docking studies showed that compound $\mathbf{A_7}$ had strong interactions with ASN34, GLN193, and GLN197 residues located in the α-helix regions of *Xoo*FtsZ. The present study demonstrates the development of FtsZ inhibitors can serve as agents to control *Xoo*-induced infections.

Keywords

43 Rice bacterial blight, diacylhydrazine derivatives, FtsZ inhibitor, antibacterial assay

44 **1. Introduction**

45 *Xanthomonas oryzae* pv. *oryzae* (*Xoo*) is a notorious pathogenic Gram-negative
46 bacterium that can invade a wide range of plant hosts, including gramineous plants
47 (such as rice, *Zizania aquatica,* and *Cenchrus ciliaris*) and cyperaceae plants (such as
48 *Cyperus difformis* and *Cyperus rotundus*).[1,2] Once infected by *Xoo*, plants develop
49 bacterial diseases with noticeable symptoms, such as anomalous growth, leaf blight,
50 and necrosis.[1,2] The well-known rice bacterial leaf blight is caused by the invasion of
51 *Xoo* and has become a major disease of rice worldwide. This intractable disease can
52 reduce rice yield by 80% at conditions that improve the pathogen's dissemination and
53 reproduction, severely threatening food security.[3-5] At present, chemical control has
54 contributed considerably in mitigating *Xoo*-induced diseases. However, few
55 agrochemicals have been found to effectively prevent and eliminate these *Xoo*-
56 induced diseases.[6-8] The commonly applied bactericides in China are bismerthiazol
57 (**BT**) and thiodiazole copper (**TC**), which date back to 1970s and 2002, respectively
58 (Figure 1). The long-term usage of common bactericides has led to the isolation of
59 **BT**- and **TC**-resistant *Xoo* strains, making the treatment of *Xoo* infections
60 challenging.[9-12] Given the abovementioned situation, highly efficient antibacterial
61 agents must be energetically pursued and developed.

62 (Insert Figure 1)

63 Designing novel antibacterial compounds on the basis of the potential targets
64 from *Xoo* may lead to the discovery of highly bioactive and innovative anti-*Xoo*
65 agents. The filamentous temperature-sensitive protein Z (FtsZ), a eukaryotic tubulin
66 homolog, is a functional and highly conserved guanosine triphosphatase (GTPase)
67 that occupies an important status in cell division.[13-15] FtsZ can preliminarily assemble
68 into single-stranded protofilaments, which subsequently form a highly dynamic "Z-

69 ring" at the prospective division site. This versatile "Z-ring" executes the functions to
70 recruit other accessory proteins for assembling the bacterial cytokinetic machinery.
71 Once this process is accomplished, the divisome constricts to facilitate the septum
72 formation and the final completion of bacterial binary division.[13-15] Therefore, FtsZ
73 has been widely studied and exploited as an identified target for creating antibacterial
74 drugs in the medicine field.[16-18] To date, a number of small-molecule inhibitors of
75 FtsZ are reported to have the ability to perturb FtsZ's polymerization and eventually
76 inhibit bacterial cell division.[19-21] Investigations have shown that natural products
77 containing the cinnamoyl or pyridinium patterns, such as curcumin, cinnamaldehyde,
78 sanguinarine, and berberine (Figure 2), show potential as FtsZ inhibitors against
79 pathogenic microorganisms.[22-31] These findings show that certain natural products can
80 serve as promising lead compounds in novel anti-FtsZ drug discovery through
81 structural optimizations. For instance, Ma and coworkers have synthesized a type of
82 cinnamaldehyde derivatives and found that compound **1** displayed potent cell division
83 inhibitory activity against *Staphylococcus aureus* ATCC25923 (Figure 2).[32] Wong et
84 al. have prepared a series of berberine-based compounds with comprehensive
85 antimicrobial activities toward clinically relevant bacteria and revealed that
86 compound **2** is an excellent FtsZ inhibitor (Figure 2).[33] Inspired by the
87 abovementioned insights, the synthesis of novel frameworks targeting *Xoo*–FtsZ may
88 supplement an effective method for managing bacterial leaf blight diseases via
89 blocking the binary division and reproduction of *Xoo*. In the present study, novel *N*-
90 (cinnamoyl)-*N*′-(substituted)acryloyl hydrazide derivatives containing the cinnamoyl
91 and pyridinium patterns were designed and synthesized by integrating these noted
92 functionalities from the abovementioned natural ingredients into a single molecular
93 architecture. These obtained derivatives were used to evaluate the anti-*Xoo* activity in

94 vitro and in vivo. Next, the GTPase activity test of recombinant *Xoo*FtsZ, *Xoo*FtsZ
95 assembly, and *Xoo* morphological changes triggered by target compounds and
96 docking study were performed to verify whether these designed compounds are the
97 potential *Xoo*FtsZ inhibitors.

98 (Insert Figure 2)

99 **2. Materials and Methods**

100 **2.1 Instruments and chemicals**

101 NMR spectra were obtained on a Bruker Biospin AG-400/500 spectrometer using
102 DMSO-d_6 as solvent and tetramethylsilane as the internal standard. HRMS spectra
103 were obtained on Thermo Scientific UltiMate 3000 spectrometer (Waltham, USA).
104 TEM images were obtained on a FEI Talos F200C electron microscope (FEI, USA)
105 operating at a voltage of 200 kV. Fluorescent *Xoo* cells were observed under an
106 Olympus-BX53-microscope (Olympus, Japan). Fluorescence spectra were obtained
107 on a FluoroMax®-4P (HORIBA Scientific, Paris, France). The CD spectrum was
108 recorded on a JASCO J-1500 spectropolarimeter (JASCO corporation, Japan). Ni-
109 NTA column and HiTrap desalting column were purchased from GE Healthcare
110 (USA). Trans-cinnamic acid and with its relative derivatives were purchased from
111 Aladdin Industrial Inc. (Shanghai, China). IPTG (isopropyl β-D-thiogalactoside),
112 HEPES, EDTA, imidazole, and NaCl were purchased from Bioengineering Co., Ltd
113 (Shanghai, China). GTP was purchased from ThermoFisher Scientific vendor (Agent:
114 Energy Chemical of Saen Chemical Technology (Shanghai) Co., Ltd., China).

115 **2.2 In vitro and in vivo anti-*Xoo* assays**

116 The in vitro anti-*Xoo* activity's evaluation of all target compounds using the
117 turbidimetric test and in vivo trials of compounds $\mathbf{A_7}$ and $\mathbf{A_8}$ against rice bacterial leaf
118 blight followed our reported methods.[11,12] Statistical analysis was executed by

119 ANOVA with software SPSS 20.0. Different uppercase letters following the control
120 efficiency values indicate that there is significant difference ($P < 0.05$) among
121 different treatment groups. The detailed calculation results could be found in
122 supporting information.

123 **2.3 Construction and purification of recombinant *Xoo*-FtsZ**

124 The sequence of *Xoo*FtsZ gene was obtained from NCBI database. The forward
125 primer *Nde*I was (5'-GGCCCCAAGGGGTTATGCTAGT-3') and the reverse primer
126 *Hind*III was (5'-GATCCCGCGAAATTAATACG-3'). The PCR fragment was
127 digested with *Nde*I and *Hind*III and ligated into the vector pET30(+) cleaved with the
128 same enzymes. To obtain the *Xoo*FtsZ, BL21Gold(DE3) pLysS strain cells
129 transformed with pET30(+) were incubated at 37℃ in LB medium until $OD_{595} = 0.6$.
130 Then, these cells were induced by supplementing 0.5 mM IPTG and subsequently
131 incubated for another 14 h at 16℃. The cells were harvested by centrifugation (3000×
132 g, 10 min, 4℃) and then were sonicated in two kinds of ice-cold binding buffers (20
133 mM phosphate (pH 7.4), 500 mM NaCl, 30 mM imidazole, 1 mM EDTA and 1 mM
134 dithiothreitol for the fluorescent titration experiment; 50 mM HEPES-KOH (pH 7.4),
135 500 mM NaCl, 30 mM imidazole, 1 mM EDTA and 1 mM dithiothreitol for the
136 GTPase activity test). After that, the supernatant was gathered by centrifugation
137 (11000×g, 10 min, 4℃). 10His-*Xoo*FtsZ was purified by a Ni-NTA column and eluted
138 with a linear gradient of 30–600 mM imidazole. The protein solution was collected,
139 and desalted by desalting column (5 × 5 mL HiTrap Desalting column, GE
140 Healthcare, USA). The final protein concentration was determined by using a protein
141 determination kit (BCA kit; Boster Biological Technology Co., Ltd., China) according
142 to the protocol of the manufacturer. Corresponding experimental results could be

143 found in Figure S1 in supporting information.

144 **2.4 Measurement of GTPase activity of *Xoo*FtsZ**

145 The GTPase activity was expressed by measurement of the amount of Pi released
146 during the assembly of *Xoo*FtsZ using a standard Malachite Green assay referred to in
147 reported methods.[26,34-35] Briefly, *Xoo*FtsZ (6 μM) was incubated without or with
148 different concentrations of target compounds in 50 mM HEPES-KOH buffer (pH 8.0)
149 containing 50 mM KCl on ice for 10 min. Then, 2.5 mM $MgCl_2$ and 1.25 mM GTP
150 were added to the reaction mixture and incubated at 28℃ to start the hydrolysis
151 reaction for 20 min. After that, 50 μL samples were quenched by the addition of 5 μL
152 acid solution at 25℃ for 10 min. Then, 15 μL malachite green solution was added to
153 the samples and incubated at 25℃ for 20 min in the dark. Finally, the Pi release was
154 determined by measuring the absorption at 620 nm. Meanwhile, the background was
155 subtracted from all the readings, and a phosphate standard curve was detected by the
156 malachite green phosphate assay kit as standard (Cayman chemical, USA). All the
157 solutions were prepared in deionized water, and compound's stock solutions were
158 prepared in DMSO and the percentage of DMSO was maintained at 0.25% for all the
159 experiments.

160 **2.5 FtsZ assembly affected by target compounds via TEM**

161 *Xoo*FtsZ (20 μM) was incubated without or with different concentrations (0 μM, 100
162 μM and 200 μM) of $\mathbf{A_7}$ in 50 mM HEPES-KOH buffer (pH 8.0) containing 50 mM
163 KCl, 1.25 mM GTP and 2.5 mM $MgCl_2$ for 5 min at 28℃. The formed FtsZ
164 aggregations were transferred to Formvar-carbon-coated copper grids, negatively
165 stained with 1% phosphotungstic acid and observed under a transmission electron
166 microscope.

167 **2.6 Measurement of the dissociation constant for compounds-*Xoo*FtsZ**

168 **interaction**

169 The dissociation constants between *Xoo*FtsZ and **A7** or berberine were determined by
170 fluorimetric titration assays.[36-38] Briefly, 20 μM FtsZ was mixed with tested
171 compounds with various concentrations (0, 5.0, 10.0, 15.0, 20.0, 25.0, 30.0, 35.0,
172 40.0, 45.0, and 50.0 μM). Then, these samples were monitored on the FluoroMax®-
173 4P instrument (Ex = 280 nm, slit widths = 3 nm). The binding constant (K_A) was
174 calculated by using the Stern–Volmer method (F_0 / F = 1 + Kq τ0[Q] = 1 + Ksv [Q])
175 at 336 nm.

176 **2.7 Analysis of secondary structural changes of *Xoo*FtsZ by circular dichroism**

177 *Xoo*FtsZ (0.6 μM) was incubated without or with different concentrations (0, 0.5, 1.0,
178 1.5 and 2.0 μM) of **A7** in a buffer solution (pH 7.4) containing 20 mM phosphate and
179 150 mM KCl. Then, these samples were detected by a JASCO J-1500
180 spectropolarimeter.[35]

181 **2.8 Molecular docking study with *Xoo*FtsZ**

182 The Modeller 9.20 was used for the homology modeling through multi-template
183 modeling using the crystal structure of FtsZ (PDB code: 2vaw, 1w58, 2r75, 1rlu, 2btq,
184 3cb2) as the template.[39-40] First, the gene sequence of *Xoo*FtsZ (Gene ID: 34180319)
185 was retrieved from NCBI Gene Bank and was translated to protein (Protein ID:
186 WP_011260226.1). Then, the conformation of *Xoo*FtsZ was achieved by energy
187 minimization using the GROMOS 54A7 force field. The detailed information could
188 be found in supporting information. Finally, the automated protein preparation
189 protocol was used for docking by Sybyl X 2.0.

190 **2.9 Morphological studies using transmission electron microscopy (TEM)**

191 *Xoo* cells (OD_{595}=0.1) in nutrient broth were supplemented with different
192 concentrations (0, 5×EC_{50}, 10×EC_{50}) of test compounds, and then were incubated for

193 24 h in a shaker (180 rpm, 28 ± 1℃). Finally, the *Xoo* morphologies were observed by
194 FEI Talos F200C apparatus.[8,22]

195 **2.10 Fluorescence patterns for the *Xoo* cells affected by A_7**

196 The above-mentioned *Xoo* cells (2.9) incubated with compound $\mathbf{A_7}$ were also
197 examined using a BX53 fluorescence microscope. Generally, the *Xoo* cells were fixed
198 with 7% formaldehyde for 10 min and incubated with FM™ 4-64 dye (3 mg L^{-1}) for
199 20 min and finally stained with DAPI (2 mg L^{-1}). After that, *Xoo* cells were fixed on a
200 glass slide before imaging.[22,35]

201 **2.11 The effect of compound A_7 on the expression of *Xoo*FtsZ by western blot**
202 **assay**[41-43]

203 *Xoo* cells (OD_{595} = 0.1) in nutrient broth were supplemented with different
204 concentrations (0, 5×EC_{50}, 10×EC_{50}) of compound $\mathbf{A_7}$, and then were incubated for 24
205 h in a shaker (180 rpm, 28 ± 1 ℃). After that, *Xoo* cells were harvested by
206 centrifugation (6000 rpm, 6 min, 10 °C) and washed with phosphate-buffered saline
207 (PBS, 10 mM, pH 7.2) 3 times. Next, these cells were lysed by sonication on a
208 VCX150 (Sonics) instrument under an ice-bath, and separated by centrifugation (12
209 000 rpm, 30 min, 4 ℃). Finally, the supernatant was determined by the BCA kit,
210 which was further adjusted to 0.30 mg/mL by dilution with the same PBS and stored
211 at −80 °C until use. The protein extracts (4.8 μg) were took and denatured in SDS
212 buffer and separated by SDS-PAGE. Then, the SDS gel was transferred onto a PVDF
213 membrane (Bio-Rad), which was further blocked in 5% nonfat dried milk solution for
214 overnight. After washing with PBST (10 mM PBS containing 0.05% Tween 20, pH
215 7.2), the one membrane was incubated with primary rabbit polyclonal anti-*Xoo*FtsZ
216 antibody (Wuhan Gene Create Biological Engineering Co., Ltd., with 1:2000 dilution
217 in 5% milk in PBST) for 2 h at 4 °C, and further washed by the same PBST.

218 Subsequently, goat anti-rabbit immunoglobulin G (IgG) HRP conjugated secondary
219 antibody (Bio-Rad, #170-6515, with 1:2000 dilution in 5% nonfat dried milk PBST
220 solution) was added, and the membrane was incubated at 4 °C for 2 h. Another
221 protein membrane was incubated with primary mouse anti-RNA polymerase (anti-
222 RNAP) antibody (Biolegend, #663104, with 1:2000 dilution in 5% milk in PBST) for
223 2 h at 4 °C, and further washed by the same PBST. Subsequently, goat anti-mouse
224 immunoglobulin G (IgG) HRP conjugated secondary antibody (CoWin Bioscience,
225 #CW0102S, with 1:5000 dilution in 5% nonfat dried milk PBST solution) was added,
226 and the membrane was incubated at 4 °C for 2 h. Finally, the membrane was washed
227 by PBST, and signals were visualized by ECL western blotting detection reagents
228 (Bio-Rad, #170-5060) using the ChemiDoc™ MP imaging system (Bio-Rad, USA).

229 **3. Results and Discussion**

230 **3.1 Synthesis and in vitro anti-*Xoo* activity of target compounds A_1–A_8**

231 The synthetic route designed to acquire target compounds **A_1-A_8** is outlined in Figure
232 3. Cinnamic acid was treated with hydrazine hydrate followed by (*E*)-3-(pyridine-3-
233 yl)acrylic acid in typical condensation reactions to provide intermediate (*E*)-*N*'-
234 cinnamolyl-3-(pyridine-3-yl)acrylhydrazide, which was then substituted by a series of
235 halogenated saturated linear alkanes to provide the target compounds **A_1-A_8**. These
236 structures were confirmed by nuclear magnetic resonance analysis and high-resolution
237 mass spectrometry (Supporting Information). The in vitro anti-*Xoo* activity showed
238 that compounds **A_2–A_8** had noticeable inhibition effects with EC_{50} values of 24.0,
239 21.0, 7.20, 2.98, 2.93, 0.99, and 2.60 mg L^{-1}, respectively (Table 1). Compound **A_7**
240 (0.99 mg L^{-1}), which had an undecyl tail, exerted the best in vitro antibacterial
241 potency. This potency was better than those of cinnamaldehyde (27.5 mg L^{-1}),
242 cinnamic acid (> 50 mg L^{-1}), curcumin (> 50 mg L^{-1}), berberine (1.56 mg L^{-1}), **TC**

243 (113 mg L^{-1}), and **BT** (37.5 mg L^{-1}), indicating that the suitable ratio of
244 hydrophobicity/hydrophilicity of a molecule can improve the exertion of antibacterial
245 performance. Their minimum inhibitory concentration (MIC) values were also
246 determined. The result showed that compounds $\mathbf{A_5}$-$\mathbf{A_8}$ displayed good inhibitory
247 effects towards *Xoo* with MIC values of 6.25, 3.13, 3.13, 3.13 mg L^{-1}, respectively.
248 This outcome agreed with the trend of EC_{50} values. The molecular docking studies of
249 *Xoo*FtsZ with A series of compounds $\mathbf{A_1}$-$\mathbf{A_8}$ were performed to benefit and promote
250 the discovery of optimal target compounds fitting into the binding site, and the
251 docking scores were provided in Table S1. The docking result showed that the
252 interplay between target compounds and *Xoo*FtsZ was certainly affected by the
253 adjustment of the hydrophobicity/hydrophilicity ratio. Among them, compound $\mathbf{A_7}$
254 formed a stronger interaction with *Xoo*FtsZ and afforded the highest score of 10.16.
255 This outcome was in accordance with the in vitro anti-*Xoo* bioassay result.

256 (Insert Figure 3)

257 (Insert Table 1)

258 **3.2 In vitro anti-*Xoo* activity of optimized molecules $\mathbf{B_1}$–$\mathbf{B_{15}}$ and $\mathbf{C_1}$**

259 Further optimization was performed on the basis of the framework of compound
260 $\mathbf{A_7}$. Consequently, compounds $\mathbf{B_1}$–$\mathbf{B_{15}}$, which had diverse substituted cinnamoyl
261 patterns or (heterocyclic substituted)acryloyl moieties (Figure 4), were designed and
262 prepared to explore highly bioactive molecules. However, these compounds displayed
263 reduced antibacterial activity compared with that of compound $\mathbf{A_7}$ (0.99 mg L^{-1}) and
264 provided EC_{50} values of 3.95–24.0 mg L^{-1} (Table 2). This outcome suggested an
265 additional substituted group on the benzene ring or the replacement of the benzene
266 ring by heterocyclic substitutes restricted the anti-*Xoo* action. The structure–activity
267 relationship was summarized as follows. (1) The chlorine atom at the meta-position

268 exerted better bioactivity, i.e., **B_4** (3-Cl, 3.95 mg L^{-1}) > **B_2** (2-Cl, 6.58 mg L^{-1}) > **B_8**
269 (4-Cl, 24.0 mg L^{-1}). (2) A strong electron-withdrawing group reduced the bioactivity,
270 i.e., **B_1** (2-NO_2, 7.64 mg L^{-1}) < **B_2** (2-Cl, 6.58 mg L^{-1}), **B_3** (3-NO_2, 14.0 mg L^{-1}) < **B_4**
271 (3-Cl, 3.95 mg L^{-1}) or **B_5** (3-Br, 4.07 mg L^{-1}), **B_6** (4-NO_2, 9.08 mg L^{-1}) < **B_7** (4-F,
272 5.32 mg L^{-1}) or **B_9** (4-Br, 5.07 mg L^{-1}). (3) The multisubstituted group showed a
273 slightly decreased bioactivity than the monosubstituted group, i.e., **B_{11}** (2,4-diCl, 8.00
274 mg L^{-1}) < **B_2** (2-Cl, 6.58 mg L^{-1}), **B_{12}** (3,4-diCl, 4.59 mg L^{-1}) < **B_4** (3-Cl, 3.95 mg
275 L^{-1}). (4) A bulky electron-donating group was unfavorable to the bioactivity, i.e., **B_{13}**
276 (3,4-diOCH_3, 16.8 mg L^{-1}) < **B_{12}** (3,4-diCl, 4.59 mg L^{-1}). Meanwhile, compounds **B_4**,
277 **B_7**, **B_9**, **B_{12}**, **B_{14}**, and **B_{15}** exerted admirable bioactivity against *Xoo* with MIC value of
278 6.25 mg L^{-1}. The compound **C_1** with the N^+ at the 4-position was fabricated (Figure 5)
279 to investigate the N^+-position toward the bioactivity and revealed a comparative anti-
280 *Xoo* capacity (EC_{50} = 1.93 mg L^{-1}, MIC = 3.13 mg L^{-1}) with that of **A_7**. Given the
281 abovementioned structural optimizations, compound **A_7** was the best anti-*Xoo*
282 molecule for further investigation.

283 (Insert Figure 4 and Figure 5)

284 (Insert Table 2)

285 **3.3 Inhibition effects of A_7 on the *Xoo*FtsZ GTPase activity**

286 The *Xoo*FtsZ GTPase activity represents an important driving force for the
287 polymerization of FtsZ. Therefore, the inhibition effect on the GTPase activity
288 triggered by compound **A_7** was evaluated. Notably, at 200 μM **A_7**, the *Xoo*FtsZ
289 GTPase activity decreased by 53.0% (Table 3), which was comparable with that of
290 berberine (53.3%). When the **A_7** dosage was decreased to 100 μM, the *Xoo*FtsZ
291 GTPase activity was reduced by 39.4%, which was higher than that of berberine
292 (25.1%). Further bioactive screening provided IC_{50} values of 171.3 μM (90.3 mg L^{-1},

293 **A_7**) and 189.4 μM (70.4 mg L^{-1}, berberine). This outcome indicated that compound
294 **A_7** can decrease the *Xoo*FtsZ GTPase activity, potentially perturbing the assembly of
295 *Xoo*FtsZ.

296 (Insert Table 3)

297 **3.4 Effect of compound A_7 on the *Xoo*FtsZ assembly**

298 The effect of compound **A_7** on the self-assembly of *Xoo*FtsZ was investigated by
299 transmission electron microscopy (TEM). In the absence of compound **A_7**, many
300 single-stranded protofilaments were observed (Figure 6a), indicating that these FtsZ
301 proteins from the phytopathogen *Xoo* possessed intrinsic polymerization properties.
302 However, the self-assembly performance was disturbed by the addition of different **A_7**
303 concentrations, consequently leading to the observation of nonlinear disorganized
304 aggregations (Figures 6b–6c). This finding was consistent with the decreased *Xoo*FtsZ
305 GTPase activity caused by the introduction of **A_7**, confirming that compound **A_7** was a
306 potential *Xoo*FtsZ inhibitor. Figure 6d shows compound **A_7** in the absence of the
307 *Xoo*FtsZ assembly.

308 (Insert Figure 6)

309 **3.5 Binding affinity between A_7 and *Xoo*FtsZ**

310 The relative binding affinity should be calculated to reveal the degree of
311 interactions between the designed compounds and *Xoo*FtsZ. As such, fluorescence
312 titration experiments were performed to calculate the binding affinity via the Stern–
313 Volmer method. The fluorescence intensity at 336 nm was gradually reduced by the
314 addition of compound **A_7** or berberine in a dose-dependent manner (Figures 7a and
315 7c), indicating that certain defined interactions occurred. The related Kq and bonding
316 constant (K_A) values are provided in Table 4. Notably, the Kq values for compound
317 **A_7** and berberine with *Xoo*FtsZ were 8.976×10^{11} M^{-1} S^{-1} and 1.736×10^{12} M^{-1} S^{-1},

318 respectively. These results were higher than that of the maximum scatter collision
319 quenching constant (2.0×10^{10} M^{-1} S^{-1}), indicating that the quenching mechanism
320 between *Xoo*FtsZ and compound $\mathbf{A_7}$ was due to the formation of a noncovalent static
321 complex rather than a dynamic collision.[36-38] Subsequently, the K_A for *Xoo*FtsZ–$\mathbf{A_7}$
322 was calculated as $10^{3.46}$ M^{-1} on the basis of the equation ($\log (F_0-F) / F = K_A + n\log$
323 $[Q]$), which was slightly lower than that of *Xoo*FtsZ–berberine ($10^{3.58}$ M^{-1}).
324 Moreover, a 1:1 binding mode was revealed between compound $\mathbf{A_7}$ and *Xoo*FtsZ
325 (Table 4), implying that compound $\mathbf{A_7}$ may be located at the crucial binding site of
326 *Xoo*FtsZ. Simultaneously, the CD spectral analysis on the secondary structure of
327 *Xoo*FtsZ suggested that compound $\mathbf{A_7}$ mostly affected the *α*-helix structure (208 nm, a
328 distinct change) of *Xoo*FtsZ (Figure 8).

329 (Insert Figure 7, Table 4, and Figure 8)

330 **3.6 Molecular Docking Simulation of A_7 with *Xoo*FtsZ**

331 The 3D structure of the *Xoo*FtsZ was established using multi-templated
332 homology modeling based on the reported crystal structures of FtsZ (PDB code:
333 2vaw, 1w58, 2r75, 1rlu, 2btq, 3cb2) as the templates to predict the possible binding
334 sites of compound $\mathbf{A_7}$ toward *Xoo*FtsZ (Supporting Information). The subsequent
335 docking study was performed using the Sybyl X 2.0. As shown in Figure 9 and Figure
336 S2A, ASN34, GLN193, and GLN197 were proposed as the primary residues that
337 displayed strong hydrogen bond interactions with compound $\mathbf{A_7}$, affording the
338 corresponding hydrogen bond distances of 2.0 Å, 1.9 Å, and 1.8 Å. In addition,
339 electrostatic interactions (Figure S2B) and hydrophilic/hydrophobic interactions
340 (Figure S2C) were important for the formation of the *Xoo*FtsZ–$\mathbf{A_7}$ complex. In
341 particular, these three residues were located in the α-helix regions of *Xoo*FtsZ (Figure
342 S3), which agreed with the changes in the secondary structure from CD analysis

343 triggered by compound **A**$_7$.[25,44-45] By contrast, the molecular docking study of
344 *Xoo*FtsZ with berberine showed that although the berberine could occupy the same
345 binding pocket, only the GLN193 residue could form the hydrogen bond interaction
346 with berberine (Figures S2D-S2F), indicating a relatively weak interaction with
347 *Xoo*FtsZ, which probably attributed to the different binding mode.

348 (Insert Figure 9)

349 **3.7 Morphological studies using TEM and fluorescence microscopy (FM)**

350 Based on the abovementioned evidence, the target compounds can be potential
351 inhibitors that have the capacity to disturb the polymerization of *Xoo*FtsZ. Therefore,
352 the influence of compound **A**$_7$ on the morphology of *Xoo* cells was studied using
353 TEM and FM. As illustrated in Figure 10, certain prolonged and filamentous bacteria
354 (Figures 10b-10c) from TEM patterns were observed after incubation with different
355 dosages of **A**$_7$, indicating that this kind of target compounds can block the binary
356 division and the normal reproduction of *Xoo*. Comparing to those of FM images
357 (Figures 10d-10f) without drug treatment, increased nucleoids and lengths in *Xoo*
358 cells (Figures 10g–10l) were observed, further agreeing with the outcome from TEM
359 investigation. Statistical data found that the average cell lengths of *Xoo* (Figure S5)
360 changed from 1.97 ± 0.43 μm (0 mg L^{-1}, **A**$_7$) to 2.47 ± 0.82 μm (4.95 mg L^{-1}, **A**$_7$) and
361 2.52 ± 0.92 μm (9.90 mg L^{-1}, **A**$_7$).

362 (Insert Figure 10)

363 **3.8 The effect of compound A$_7$ on the expression of *Xoo*FtsZ by western blot**
364 **assay**

365 To investigate the effect of compound **A**$_7$ on the expression of *Xoo*FtsZ, the
366 related western blot assay was performed by a classical immunoblotting technique
367 using the anti-*Xoo*FtsZ antibody. The result showed that compound **A**$_7$ could

368 moderately reduce the expression of *Xoo*FtsZ in a dosage-dependent manner,
369 indicating that compound $\mathbf{A_7}$ not only perturbed the FtsZ self-assembly, but also
370 probably decreased the expression of *Xoo*FtsZ to block the normal binary division
371 (Figure S6).

372 **3.9 In vivo anti-*Xoo* infections in rice**

373 The designed target compounds can block the binary division and the
374 reproduction of *Xoo* by targeting the *Xoo*FtsZ, which may provide an effective
375 method for managing bacterial leaf blight diseases. Therefore, the in vivo anti-*Xoo*
376 infections in rice should be evaluated. Compounds $\mathbf{A_7}$ and $\mathbf{A_8}$ exerted good curative
377 activities (63.2% and 57.1%, respectively, Table 5 and Figure 11) for reducing rice
378 bacterial leaf blight. These data indicate that title compounds can be used for
379 managing bacterial diseases by targeting the FtsZ of phytopathogens. Moreover, this
380 type of target molecules showed low phytotoxicity against rice plants.

381 (Insert Figure 11 and Table 5)

382 An array of novel *N*-(cinnamoyl)-*N*′-(substituted)acryloyl hydrazide derivatives
383 containing cinnamoyl and pyridinium moieties were prepared to explore novel
384 antibacterial compounds against *Xoo*-induced infections directed by targeting FtsZ
385 from *Xoo*. Bioassay results showed that compound $\mathbf{A_7}$ had an excellent anti-*Xoo*
386 activity (EC_{50} = 0.99 mg L^{-1}, MIC = 3.13 mg L^{-1}) in vitro and distinct curative
387 activity (63.2% at 200 mg L^{-1}) in vivo. Investigations found that compound $\mathbf{A_7}$ can
388 reduce the GTPase activity of recombinant *Xoo*FtsZ and subsequently disturb the self-
389 assembly and polymerization of *Xoo*FtsZ from TEM images. The binding constant
390 between compound $\mathbf{A_7}$ and *Xoo*FtsZ was calculated as $10^{3.46}$ M^{-1} by using
391 fluorescence titration. The docking study displayed that compound $\mathbf{A_7}$ had strong
392 interactions with ASN34, GLN193, and GLN197 residues located in the α-helix

regions of *Xoo*FtsZ. Moreover, prolonged and filamentous bacteria were observed in TEM and FM images after incubation with compound $\mathbf{A_7}$, indicating that the target compounds impede the binary division and normal reproduction of *Xoo*. In addition, compound $\mathbf{A_7}$ probably also decreased the expression of *Xoo*FtsZ to block the binary division. The abovementioned evidence validated that the designed compounds were potential FtsZ inhibitors against the phytopathogen *Xoo*. The present study can stimulate the development of more potent FtsZ inhibitors as interchangeable agents to manage *Xoo*-induced infections.

Abbreviations

FtsZ, filamentous temperature-sensitive protein Z; *Xoo*, *Xanthomonas oryzae* pv. *oryzae*; HRMS, high-resolution mass spectrometry; TEM, transmission electron microscope; FM, fluorescence microscopy; MIC, minimum inhibitory concentration.

Acknowledgements

We acknowledge the National Natural Science Foundation of China (21877021, 21702037, 31860516, 21662009), the Research Project of Ministry of Education of China (20135201110005, 213033A), and Guizhou Provincial S&T Program ([2017]5788), Program of Introducing Talents of Discipline to Universities of China (111 Program, D20023).

Supporting Information

Supplementary data including Determination of minimum inhibitory concentration; homologous modeling; purification of the recombinant *Xoo*FtsZ (Figure S1); The docking scores of compounds $\mathbf{A_1}$-$\mathbf{A_8}$ and berberine with *Xoo*FtsZ (Table S1); predicted binding modes of *Xoo*FtsZ with compound $\mathbf{A_7}$ (Figure S2); predicted secondary structure of *Xoo*FtsZ (Figure S3); TEM images for *Xoo* after incubation with different control compounds (Figure S4); Statistical data of the lengths of *Xoo*

418 cells from TEM images after incubation with different concentrations of compound
419 **A**$_7$ (Figure S5); the effect of compound **A**$_7$ on the expression of *Xoo*FtsZ by western
420 blot (Figure S6); general synthetic procedures and experimental characterization data;
421 NMR and HRMS spectra for the target compounds (Figures S7−S80).

422 **Conflict of interest**

423 The authors declare no competing financial interest.

424 **References**

425 1. Saha, S.; Garg, R.; Biswas, A.; Rai, A. B. Bacterial diseases of rice: an overview.
426 *J. Pure Appl Microbiol.* **2015**, *9*, 725-736.
427 2. Kim, S. M.; Suh, J. P.; Qin, Y.; Noh, T. H.; Reinke, R. F.; Jena, K. K.
428 Identification and fine-mapping of a new resistance gene, *Xa40*, conferring
429 resistance to bacterial blight races in rice (*Oryza sativa L.*). *Theor. Appl. Genet*.
430 **2015**, *128*, 1933-1943.
431 3. Shen, Y. W.; Ronald, P. Molecular determinants of disease and resistance in
432 interactions of *Xanthomonas oryzae pv. oryzae* and rice. *Microbes Infect*. **2002**,
433 *4*, 1361-1367.
434 4. Mansfield, J.; Genin, S.; Magori, S.; Citovsky, V.; Sriariyanum, M.; Ronald, P.;
435 Dow, M.; Verdier, V.; Beer, S. V.; Machado, M. A.; Toth, I.; Salmond, G.;
436 Foster, G. D. Top 10 plant pathogenic bacteria in molecular plant pathology.
437 *Mol. Plant Pathol*. **2012**, *13*, 614-629.
438 5. Nino-Liu, D. O.; Ronald, P. C.; Bogdanove, A. J. *Xanthomonas oryzae*
439 pathovars: model pathogens of a model crop. *Mol. Plant Pathol*. **2006**, *7*, 303-
440 324.
441 6. Li, P.; Tian, P. Y.; Chen, Y. Z.; Song, X. P.; Xue, W.; Jin, L. H.; Hu, D. Y.;
442 Song, B. A. Novel bisthioether derivatives containing a 1, 3, 4-oxadiazole
443 moiety: design, synthesis, antibacterial and nematocidal activities. *Pest Manag.*
444 *Sci*. **2018**, *74*, 844-852.
445 7. Li, P.; Hu, D. Y; Xie, D. D.; Chen, J. X.; Jin, L. H.; Song, B. A. Design,
446 synthesis, and evaluation of new sulfone derivatives containing a 1, 3, 4-
447 oxadiazole moiety as active antibacterial agents. *J. Agric. Food Chem*. **2018**, *66*,
448 3093-3100.

449 8. Wang, P. Y.; Wang, M. W.; Zeng, D.; Xiang, M.; Rao, J. R.; Liu, Q. Q.; Liu, L.
450 W.; Wu, Z. B.; Li, Z.; Song, B. A.; Yang, S. Rational optimization and action
451 mechanism of novel imidazole (or imidazolium)-labeled 1, 3, 4-oxadiazole
452 thioethers as promising antibacterial agents against plant bacterial diseases. *J.*
453 *Agric. Food Chem*. **2019**, *67*, 3535-3545.
454 9. Zhu, X. F.; Xu, Y.; Peng, D.; Zhang, Y.; Huang, T. T.; Wang, J. X.; Zhou, M. G.
455 Detection and characterization of bismerthiazol-resistance of *Xanthomonas*
456 *oryzae pv. oryzae*. *Crop Prot*. **2013**, *47*, 24-29.
457 10. Shen, G. B.; Zhou, M. G. Biological properties of resistant mutants of
458 *Xanthomonas oryzae* to Saikuzuo. *J. Nanjing Agric. Univ*. **2001**, *24*, 33-36.
459 11. Zhao, Y. L.; Huang, X.; Liu, L. W.; Wang, P. Y.; Long, Q. S.; Tao, Q. Q.; Li, Z.;
460 Yang, S. Identification of racemic and chiral carbazole derivatives containing an
461 isopropanolamine linker as prospective surrogates against plant pathogenic
462 bacteria: in vitro and in vivo assays, and quantitative proteomics. *J. Agric. Food*
463 *Chem.* **2019**, *67*, 7512-7525.
464 12. Wang, P. Y.; Zhou, L.; Zhou, J.; Wu, Z. B.; Xue, W.; Song, B. A.; Yang, S.
465 Synthesis and antibacterial activity of pyridinium-tailored 2, 5-substituted-1, 3,
466 4-oxadiazole thioether/sulfoxide/sulfone derivatives. *Bioorg. Med. Chem. Lett*.
467 **2016**, *26*, 1214-1217.
468 13. Oliva, M. A.; Cordell, S. C.; Löwe, J. Structural insights into FtsZ protofilament
469 formation. *Nat. Struct. Mol. Biol.* **2004**, *11*, 1243-1250.
470 14. Margolin, W. FtsZ and the division of prokaryotic cells and organelles. *Nat. Rev.*
471 *Mol. Cell Bio.* **2005**, *6*, 862-871.

472 15. Li, Y.; Hsin, J.; Zhao, L. Y.; Cheng, Y. W.; Shang, W. N.; Huang, K. C.; Wang,
473 H. W.; Ye, S. FtsZ protofilaments use a hinge-opening mechanism for
474 constrictive force generation. *Science* **2013**, *341*, 392-395.
475 16. Huang, Q.; Tonge, P. J.; Slayden, R. A.; Kirikae, T.; Ojima, I. FtsZ: a novel
476 target for tuberculosis drug discovery. *Curr. Top. Med. Chem.* **2007**, *7*, 527-543.
477 17. Sass, P.; Brötz-Oesterhelt, H. Bacterial cell division as a target for new
478 antibiotics. *Curr. Opin. Microbio.* **2013**, *16*, 522-530.
479 18. Panda, D.; Bhattacharya, D.; Gao, Q. H.; Oza, P. M.; Lin, H. J.; Hawkins, B.;
480 Hibbs, D. E.; Groundwater, P. W. Identification of agents targeting FtsZ
481 assembly. *Future Med. Chem.* **2016**, *8*, 1111-1132.
482 19. Schaffner-Barbero, C.; Martín-Fontecha, M.; Chacón, P.; Andreu, J. M.
483 Targeting the assembly of bacterial cell division protein FtsZ with small
484 molecules. *ACS Chem. Bio.* **2012**, *7*, 269-277.
485 20. Hurley, K. A.; Santos, T. M.; Nepomuceno, G. M.; Huynh, V.; Shaw, J. T.;
486 Weibel, D. B. Targeting the bacterial division protein FtsZ. *J. Med. Chem.* **2016**,
487 *59*, 6975-6998.
488 21. Kusuma, K. D.; Payne, M.; Ung, A. T.; Bottomley, A. L.; Harry, E. J. FtsZ as an
489 Antibacterial Target: Status and Guidelines for Progressing This Avenue. *ACS*
490 *Infect. Dis.* **2019**, *5*, 1279-1294.
491 22. Tushar, K.; Beuria, M. K.; Panda. D. Sanguinarine blocks cytokinesis in bacteria
492 by inhibiting FtsZ assembly and bundling. *Biochemistry* **2005**, *44*, 16584-16593.
493 23. Huang, Q.; Kirikae, F.; Kirikae, T.; Pepe, A.; Amin, A.; Respicio, L.; Slayden,
494 R. A.; Tonge, P.; Ojima, I. Targeting FtsZ for antituberculosis drug discovery:
495 noncytotoxic taxanes as novel antituberculosis agents. *J. Med. Chem*. **2006**, *49*,
496 463-466.

497 24. Domadia, P.; Swarup, S.; Bhunia, A.; Sivaraman, J.; Dasgupta, D. Inhibition of
498 bacterial cell division protein FtsZ by cinnamaldehyde. *Biochem. Pharmacol.*
499 **2007**, *74*, 831-840.
500 25. Domadia, P. N.; Bhunia, A.; Sivaraman, J.; Swarup, S.; Dasgupta, D. Berberine
501 targets assembly of *Escherichia coli* cell division protein FtsZ. *Biochemistry*
502 **2008**, *47*, 3225-3234.
503 26. Rai, D. S.; Roy, K. J.; Panda, D. N. Curcumin inhibits FtsZ assembly: an
504 attractive mechanism for its antibacterial activity. *Biochem. J.* **2008**, *410*, 147-
505 155.
506 27. Kaur, S.; Modi, N. H.; Panda, D.; Roy, N. Probing the binding site of curcumin
507 in *Escherichia coli* and *Bacillus subtilis* FtsZ – A structural insight to unveil
508 antibacterial activity of curcumin. *Eur. J. Med. Chem*. **2010**, *45*, 4209-4214.
509 28. Plaza, A.; Keffer, J. L.; Bifulco, G.; Lloyd, J. R.; Bewley, C. A. Chrysophaentins
510 A− H, antibacterial bisdiarylbutene macrocycles that inhibit the bacterial cell
511 division protein FtsZ. *J. Am. Chem. Soc.* **2010**, *132*, 9069-9077.
512 29. Duggirala, S.; Nankar, R. P.; Rajendran, S.; Doble, M. Phytochemicals as
513 inhibitors of bacterial cell division protein FtsZ: coumarins are promising
514 candidates. *Appl. Biochem. Biotechnol.* **2014**, *174*, 283-296.
515 30. Panda, P.; Taviti, A. C.; Satpati, S.; Kar, M. M.; Dixit, A.; Beuria, T. K.
516 Doxorubicin inhibits *E. coli* division by interacting at a novel site in FtsZ.
517 *Biochem. J.* **2015**, *471*, 335-346.
518 31. Matsui, T.; Lallo, S.; Nisa, K.; Morita, H. Filamenting temperature-sensitive
519 mutant Z inhibitors from Glycyrrhiza glabra and their inhibitory mode of action.
520 *Bioorg. Med. Chem. Lett*. **2017**, *27*, 1420-1424.

521 32. Li, X.; Sheng, J.; Huang, G.; Ma, R.; Yin, F. X.; Song, D.; Zhao, C.; Ma, S. T.
522 Design, synthesis and antibacterial activity of cinnamaldehyde derivatives as
523 inhibitors of the bacterial cell division protein FtsZ. *Eur. J. Med. Chem*. **2015**,
524 *97*, 32-41.
525 33. Sun, N.; Chan, F. Y.; Lu, Y. J.; Neves, M. A.; Lui, H. K.; Wang, Y.; Chow, K.
526 Y.; Chan, K. F.; Yan, S. C.; Leung, Y. C.; Abagyan, R.; Chan, T. H.; Wong, K.
527 Y. Rational design of berberine-based FtsZ inhibitors with broad-spectrum
528 antibacterial activity. *PLoS One* **2014**, *22*, 2601-2612.
529 34. Cai, Y.; S.; Yuan, W. C.; Li, Y.; Huang, X. H.; Guo, Q.; Tang, Z. W.; .Fang, Z.
530 Y.; Lin, H.; Wong, K. Y.; Lu, Y. J.; Sun, N, Antibacterial activity of indolyl-
531 quinolinium derivatives and study their mode of action. *Bioorg. Med. Chem*.
532 **2019**, *27*, 1274-1282.
533 35. Singh, D.; Bhattacharya, A.; Rai, A.; Dhaked, H. P. S.; Awasthi, D.; Ojima, I.;
534 Panda, D. SB-RA-2001 inhibits bacterial proliferation by targeting FtsZ
535 assembly. *Biochemistry* **2014**, *53*, 2979-2992.
536 36. Bi, S.; Ding, L.;, Tian, Y.; Song, D. Q.; Zhou, X.; Liu, X.; Zhang, H. Q.
537 Investigation of the interaction between flavonoids and human serum albumin. *J.*
538 *Mol. Struct*. **2004**, *703*, 37-45.
539 37. Wang, Z. C.; Li, X. Y.; Wang, W. L.; Zhang, W. Y.; Yu, L.; Hu, D. Y.; Song, B.
540 A. Interaction research on the antiviral molecule Dufulin targeting on southern
541 rice black streaked dwarf virus P9-1 nonstructural protein. *Viruses-Basel* **2015**,
542 *7*, 1454-1473.
543 38. Ran, L. L.; Ding, Y.; Luo, L. Z.; Gan, X. H.; Li, X. Y.; Chen, Y. Z.; Hu, D. Y.;
544 Song, B. A. Interaction research on an antiviral molecule that targets the coat

545 protein of southern rice black-streaked dwarf virus. *Int. J. Biol. Macromol.* **2017**,
546 *103*, 919-930.
547 39. Buenavista, M. T.; Roche, D. B.; McGuffin, L. J. Improvement of 3D protein
548 models using multiple templates guided by single-template model quality
549 assessment. *Bioinformatics* **2012**, *28*, 1851-1857.
550 40. Jamroz, M.; Kolinski, A. Modeling of loops in proteins: a multi-method approach.
551 *BMC Struct. Biol*. **2010**, *10*, 5.
552 41. Chen, B.; Long, Q. S.; Meng, J.; Zhou, X.; Wu, Z. B.; Tuo, X. X.; Ding, Y.;
553 Zhang, L.; Wang, P. Y.; Li, Z.; Yang, S. Target discovery in *Ralstonia*
554 *solanacearum* through an activity-based protein profiling technique based on
555 bioactive oxadiazole sulfones. *J. Agric. Food Chem*. **2020**, *68*, 2340−2346
556 42. Xu, J. B.; Zhang, C. P.; Wunierbieke, M. L.; Yang, X. F.; Li, Y. L.; Chen, X. B.;
557 Chen, G. Y.; Zou, L. F. An improved protein expression system for T3SS genes
558 regulation analysis in *Xanthomonas oryzae* pv. *oryzae*. *J. Integr. Agr*. **2019**, *18*,
559 1189-1198.
560 43. Yang, N. N.; Cao, Q.; Hu, S. Y.; Xu, C. C.; Fan, K.; Chen, F. F.; Yang, C. G.;
561 Liang, H. H.; Wu, M.; Bae, T.; Lan, L. F. Alteration of protein homeostasis
562 mediates the interaction of *Pseudomonas aeruginosa* with *Staphylococcus aureus*.
563 *Mol. Microbiol*. **2020**, DOI: 10.1111/mmi.14519.
564 44. Hemaiswarya, S.; Soudaminikkutty, R.; Narasumani, M. L.; Doble, M.
565 Phenylpropanoids inhibit protofilament formation of *Escherichia coli* cell
566 division protein FtsZ. *J. Med. Microbiol*. **2011**, *60*, 1317-1325.
567 45. Elsen, N. L.; Lu, J.; Parthasarathy, G.; Reid, J. C.; Sharma, S.; Soisson, S. M.;
568 Lumb, K. J. Mechanism of action of the cell-division inhibitor PC190723:

569 modulation of FtsZ assembly cooperativity. *J. Am. Chem. Soc*. **2012**, *134*, 12342-
570 12345.
571

573 **Figure captions**

574 **Figure 1.** Chemical structures of bismerthiazol (**BT**) and thiodiazole copper (**TC**), the
575 commonly applied bactericides for managing *Xoo*-induced infections.

576 **Figure 2.** Molecular structures of natural and reported FtsZ inhibitors and the design
577 concepts for target molecules in the current work.

578 **Figure 3.** Synthetic route for the target molecules $\mathbf{A_1}$–$\mathbf{A_8}$.

579 **Figure 4.** Synthetic route for the target molecules $\mathbf{B_1}$–$\mathbf{B_{15}}$.

580 **Figure 5.** Synthetic route for the target molecule $\mathbf{C_1}$.

581 **Figure 6.** Effect of different concentrations of compound $\mathbf{A_7}$ on *Xoo*FtsZ assembly: a)
582 0 μM $\mathbf{A_7}$ + 20 μM *Xoo*FtsZ, b) 200 μM $\mathbf{A_7}$ + 20 μM *Xoo*FtsZ, c) 100 μM $\mathbf{A_7}$ + 20 μM
583 *Xoo*FtsZ, d) 200 μM $\mathbf{A_7}$ without *Xoo*FtsZ. Scale bars are 2 μm.

584 **Figure 7.** Fluorescence titration experiments of *Xoo*FtsZ (20 μM) with elevated
585 concentrations (from 0 μM to 50 μM) of $\mathbf{A_7}$ (a and b) and berberine (c and d), λ_{ex} =
586 278 nm, λ_{em} = 336 nm.

587 **Figure 8.** CD spectra of *Xoo*FtsZ (0.6 μM) after treatment with various
588 concentrations (0.5, 1.0, 1.5, and 2.0 μM) of $\mathbf{A_7}$. The troughs at 208 and 216 nm are
589 characteristics of α-helix and β-sheet, respectively, of *Xoo*FtsZ.

590 **Figure 9.** Predicted binding modes of *Xoo*FtsZ with compound $\mathbf{A_7}$.

591 **Figure 10.** TEM images of *Xoo* after incubation with (a) 0, (b) 4.95, and (c) 9.90 mg
592 L^{-1} $\mathbf{A_7}$. Scale bars are 2 μm. FM images of *Xoo* after incubation with (d, e, f) 0, (g, h,
593 i) 4.95, and (j, k, l) 9.90 mg L^{-1} $\mathbf{A_7}$. The DNA was visualized using DAPI and shown
594 in blue. (f, i, l) show the overlay of the (d, e), (g, h), and (j, k), respectively. Scale bars
595 are 5 μm.

596 **Figure 11**. Curative activity and phytotoxicity of compounds $\mathbf{A_7}$ and $\mathbf{A_8}$ against rice
597 bacterial leaf blight under greenhouse conditions at 200 mg L^{-1}.

599 **Tables**

600 **Table 1.** In vitro anti-*Xoo* activity of the target compounds $\mathbf{A_1}$–$\mathbf{A_8}$.

Compounds	*n*	Regression equation	r^2	EC_{50} (mg L^{-1})	MIC (mg L^{-1})
$\mathbf{A_1}$	4			> 50.0	> 200
$\mathbf{A_2}$	5	y = 3.507x + 0.1523	0.96	24.0 ± 1.30	100
$\mathbf{A_3}$	6	y = 3.716x − 0.0835	0.93	21.0 ± 2.60	50
$\mathbf{A_4}$	7	y = 6.032x − 0.1561	0.89	7.20 ± 0.60	12.5
$\mathbf{A_5}$	8	y = 11.155x − 0.3060	0.94	2.98 ± 0.21	6.25
$\mathbf{A_6}$	9	y = 10.997x − 0.1442	0.98	2.93 ± 0.25	3.13
$\mathbf{A_7}$	10	y = 2.8810x + 5.017	0.92	0.99 ± 0.08	3.13
$\mathbf{A_8}$	11	y = 11.745x + 0.1941	0.97	2.60 ± 0.15	3.13
Cinnamaldehyde		y = 3.3540x + 0.1735	0.85	27.5 ± 2.30	100
Cinnamic acid				> 50.0	100
Curcumin				> 50.0	> 200
Berberine		y = 2.8402x + 4.4504	0.93	1.56 ± 0.18	25
TC		y = 2.081x + 0.7280	0.99	113 ± 2.18	
BT		y = 3.8017x − 0.9885	0.99	37.5 ± 1.5	100

602 **Table 2.** In vitro anti-*Xoo* activity of the target compounds **B_1–B_{15}** and **C_1**.

Compounds	Regression equation	r^2	EC_{50} (mg L^{-1})	MIC (mg L^{-1})
B_1	y = 5.653x + 0.0042	0.97	7.64 ± 0.16	12.5
B_2	y = 4.913x + 0.9811	0.94	6.58 ± 0.12	50
B_3	y = 4.373x − 0.0127	0.99	14.0 ± 0.14	25.0
B_4	y = 2.3037x + 3.6275	0.94	3.95 ± 0.27	6.25
B_5	y = 8.2546x − 0.0324	0.99	4.07 ± 0.18	50.0
B_6	y = 4.4213x + 0.7623	0.96	9.08 ± 0.28	25.0
B_7	y = 4.1011x + 2.0184	0.92	5.32 ± 0.25	6.25
B_8	y = 5.5322x + 0.2062	0.97	24.0 ± 1.30	25.0
B_9	y = 5.3953x + 1.1831	0.97	5.07 ± 0.22	6.25
B_{10}	y = 7.7765x − 3.0668	0.97	10.9 ± 0.45	12.5
B_{11}	y = 5.5875x + 0.0257	0.98	8.00 ± 0.78	12.5
B_{12}	y = 7.6917x − 0.0916	0.97	4.59 ± 0.10	6.25
B_{13}	y = 4.1050x − 0.0302	0.99	16.8 ± 0.40	25.0
B_{14}	y = 7.3221x − 0.4669	0.97	5.58 ± 0.32	6.25
B_{15}	y = 7.2215x − 0.0347	0.99	4.96 ± 0.11	6.25
C_1	y = 4.8292x + 3.6278	0.95	1.93 ± 0.13	3.13
Cinnamaldehyde	y = 3.3540x + 0.1735	0.85	27.5 ± 2.30	100
Cinnamic acid			> 50.0	100
Curcumin			> 50.0	> 200
Berberine	y = 2.8402x + 4.4504	0.93	1.56 ± 0.18	25
TC	y = 2.081x + 0.7280	0.99	113 ± 2.18	
BT	y = 3.8017x − 0.9885	0.99	37.5 ± 1.5	100

604 **Table 3.** Inhibition effects of compound $\mathbf{A_7}$ and berberine on the *Xoo*FtsZ GTPase
605 activity.

Compounds	Inhibition rate (%)		IC_{50} (μM)
	200 μM	100 μM	
$\mathbf{A_7}$	53.0 ± 4.9	39.4 ± 2.6	171.3 ± 2.4
Berberine hydrochloride	53.3 ± 1.1	25.1 ± 4.2	189.4 ± 2.5

607 **Table 4.** Binding parameters of compound $\mathbf{A_7}$ and berberine with *Xoo*FtsZ.

Compounds	Stern–Volmer quenching constants			Binding parameters		
	Ksv (M^{-1})	Kq (M^{-1} S^{-1})	R	K_A (M^{-1})	n	R^2
$\mathbf{A_7}$	8.976×10^3	8.976×10^{11}	0.99	$10^{3.46}$	0.89	0.98
Berberine	1.736×10^4	1.736×10^{12}	0.97	$10^{3.58}$	0.86	0.87

609 **Table 5.** Curative activity of compounds $\mathbf{A_7}$ and $\mathbf{A_8}$ against rice bacterial leaf blight at
610 200 mg L^{-1} under greenhouse conditions.

Treatments	14 days after inoculation		
	Morbidity (%)	Disease index (%)	Control Efficiency (%)[b]
$\mathbf{A_7}$	100	35.2	63.2A
$\mathbf{A_8}$	100	41.0	57.1A
Thiodiazole copper	100	55.6	41.8B
CK[a]	100	95.6	/

611 [a]Negative control. [b]Statistical analysis was conducted using ANOVA under the condition of equal
612 variances assumed ($p > 0.05$) and equal variances not assumed ($p < 0.05$). Different uppercase
613 letters indicate the values of curative activity with significant difference among different treatment
614 groups at $p < 0.05$.

616 **Figures**

617 **Figure 1.**

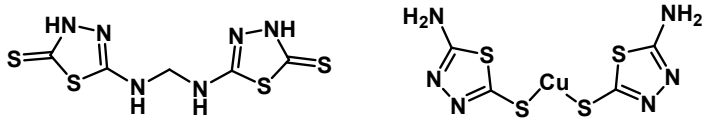

618 Bismerthiazol Thiodiazole copper

620 **Figure 2.**

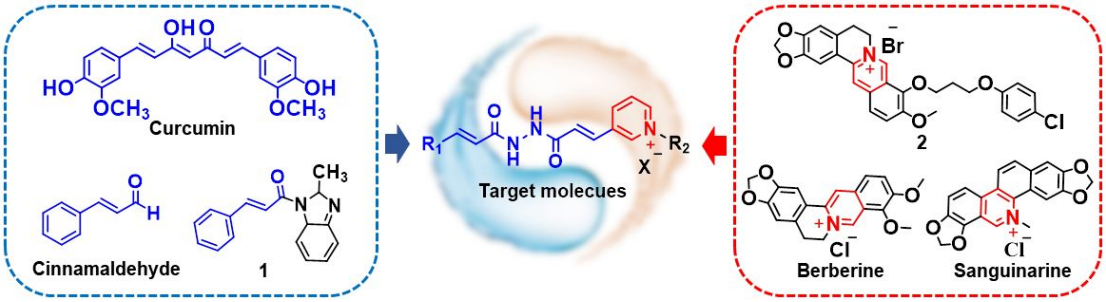

621

623 **Figure 3.**

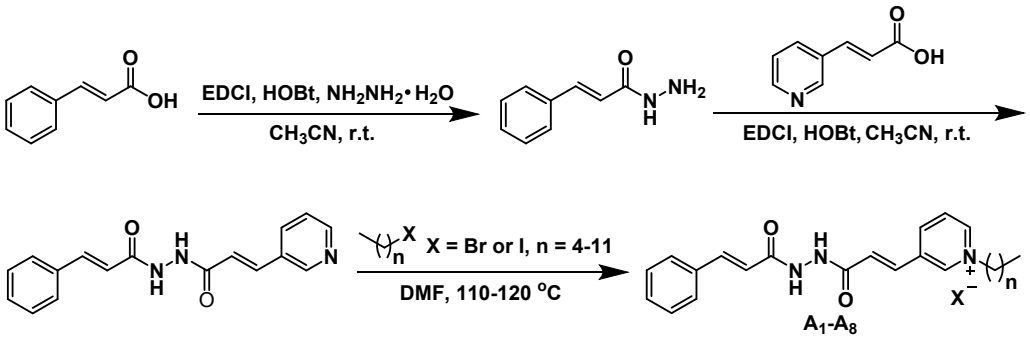

624

626 **Figure 4.**

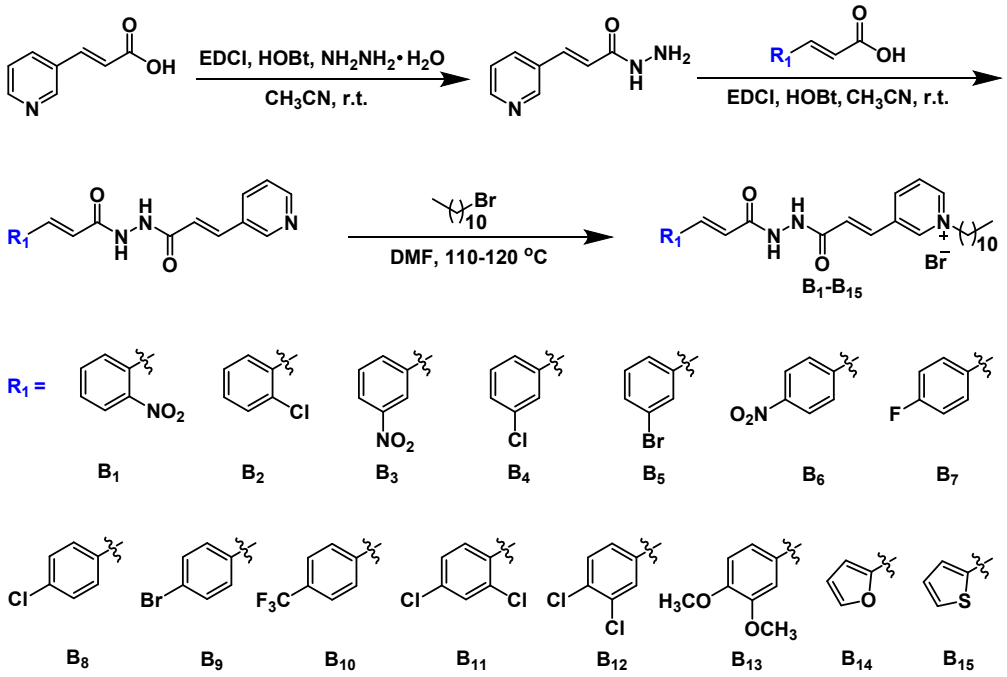

627

629 **Figure 5.**

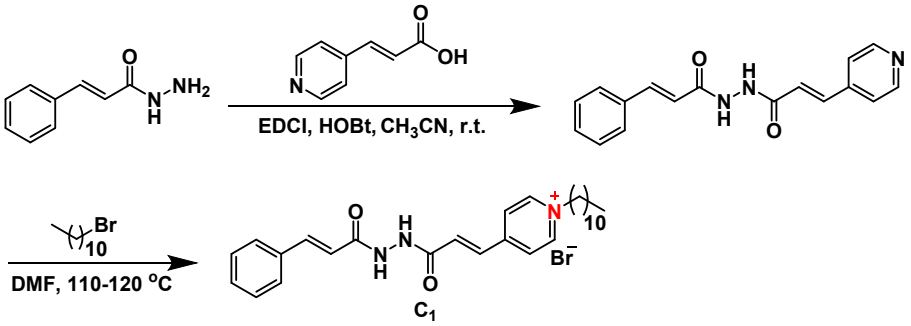

630

632 **Figure 6.**

633 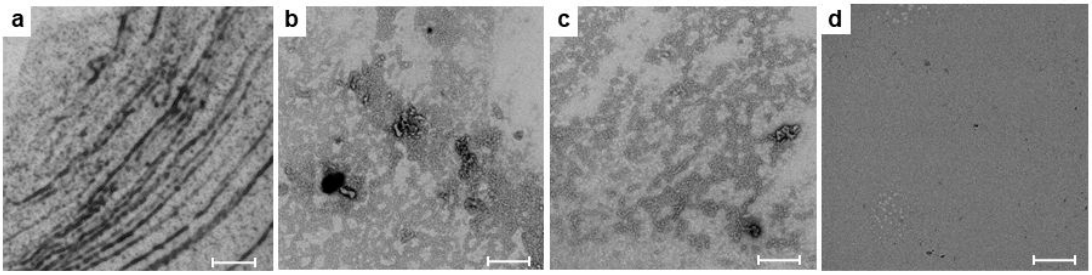

Figure 7.

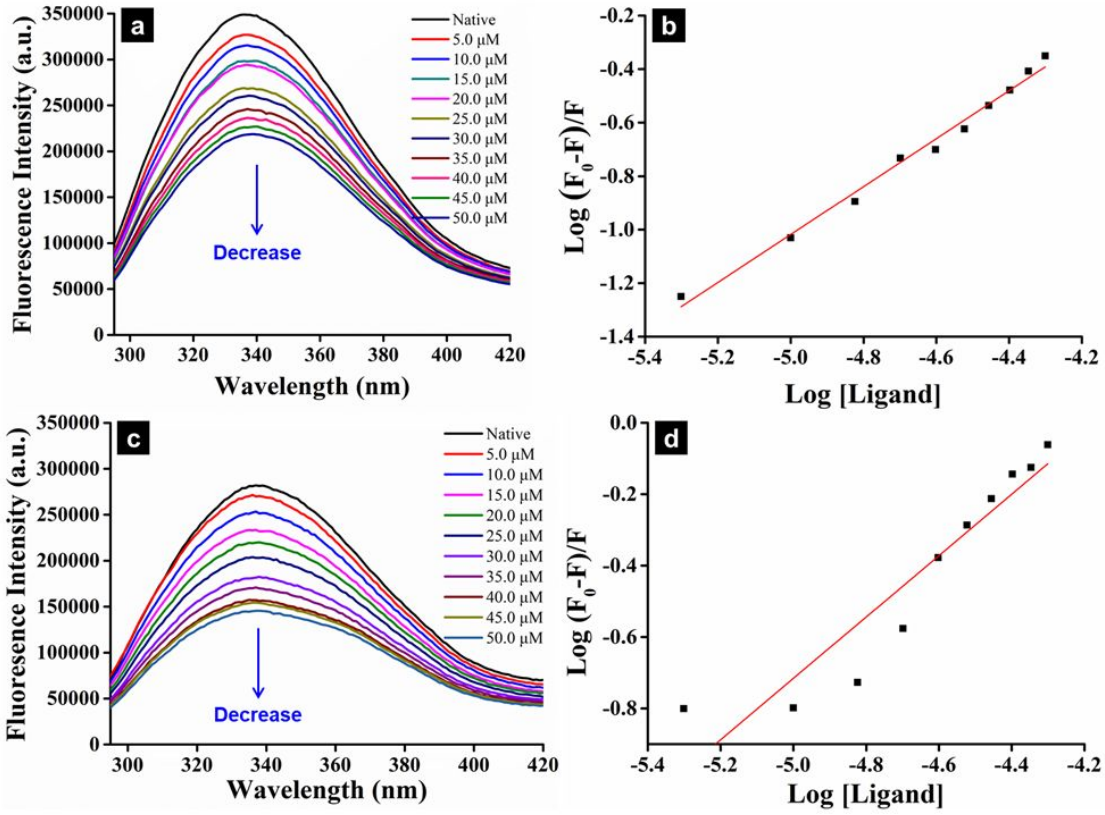
a
Fluorescence Intensity (a.u.)
Wavelength (nm)
Decrease
Native
5.0 μM
10.0 μM
15.0 μM
20.0 μM
25.0 μM
30.0 μM
35.0 μM
40.0 μM
45.0 μM
50.0 μM
b
Log (F0-F)/F
Log [Ligand]
c
Fluorescence Intensity (a.u.)
Wavelength (nm)
Decrease
d
Log (F0-F)/F
Log [Ligand]

638 **Figure 8.**

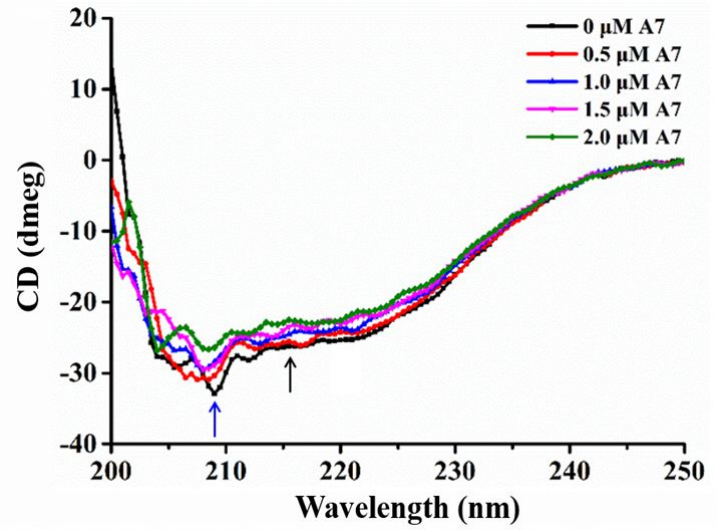

639

641 **Figure 9.**

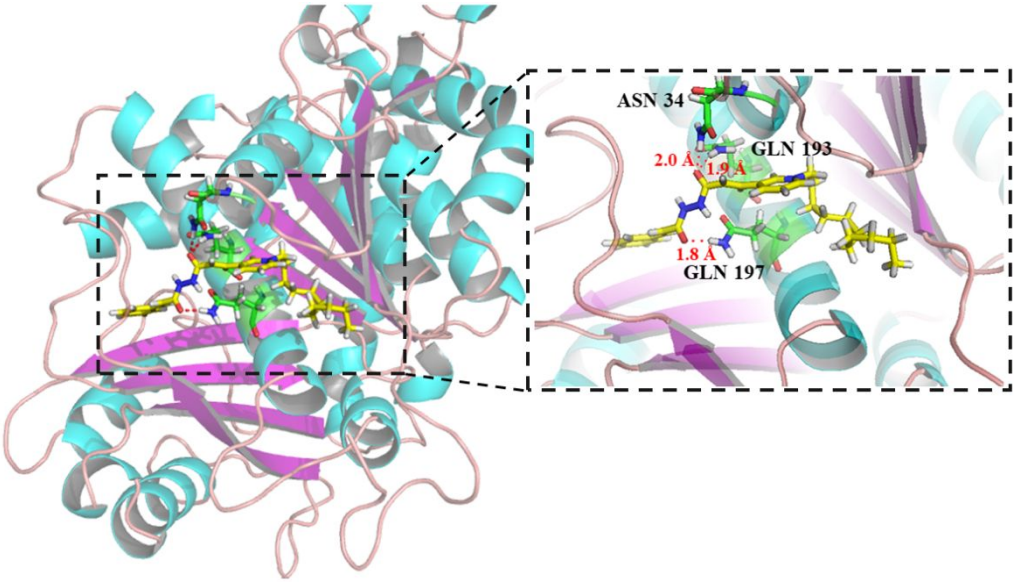

642

Figure 10.

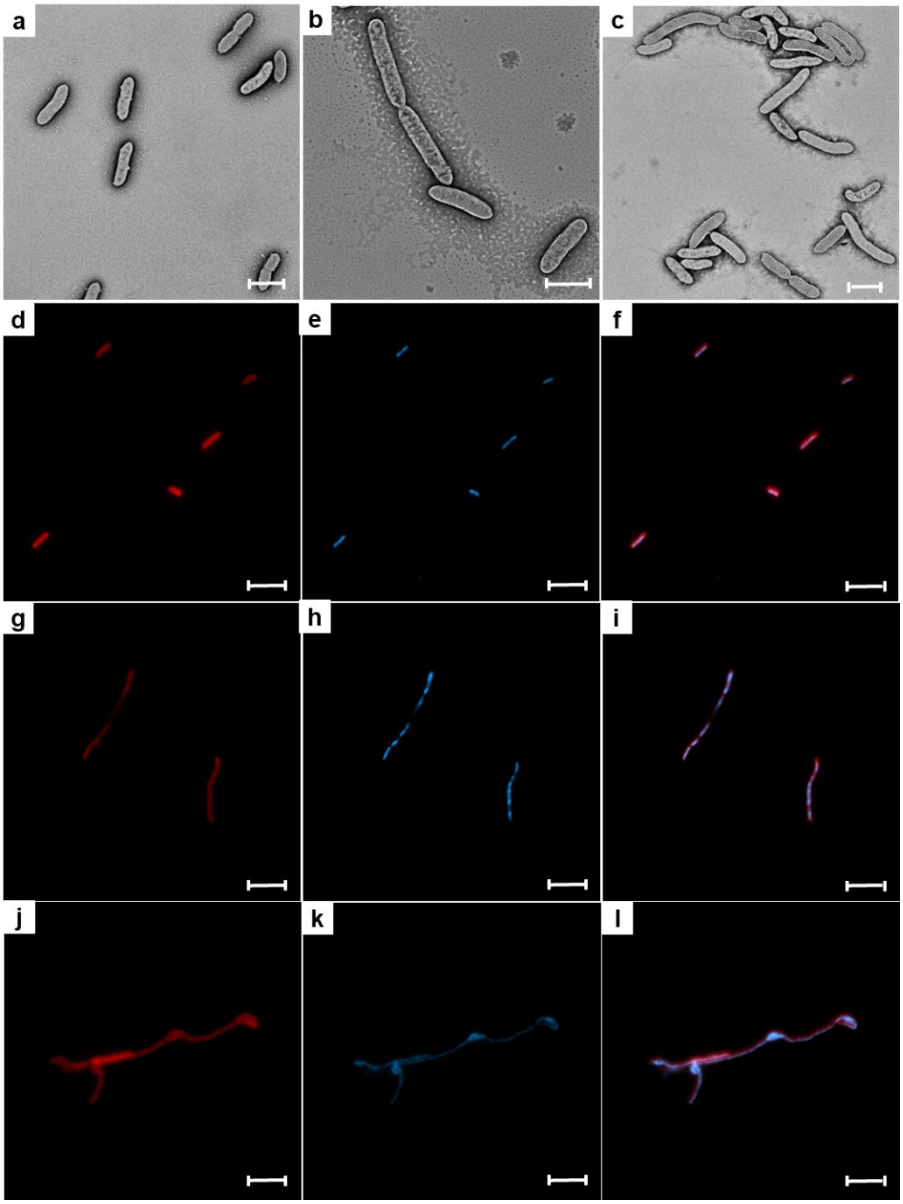

647 **Figure 11.**

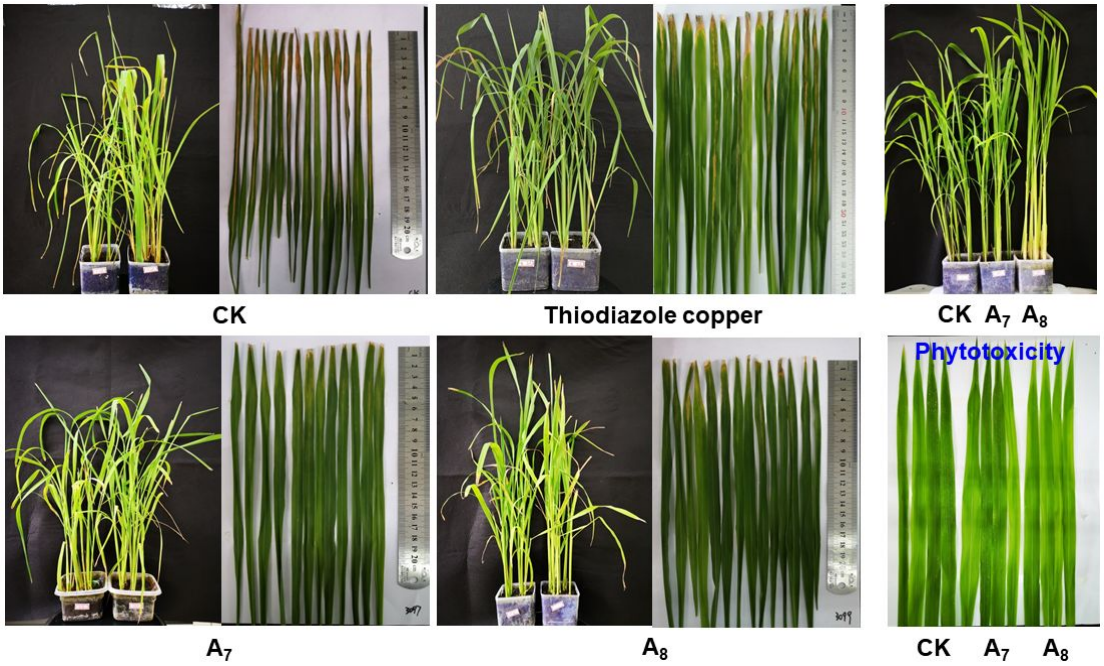

648

650 **Graphic for Table of Contents**

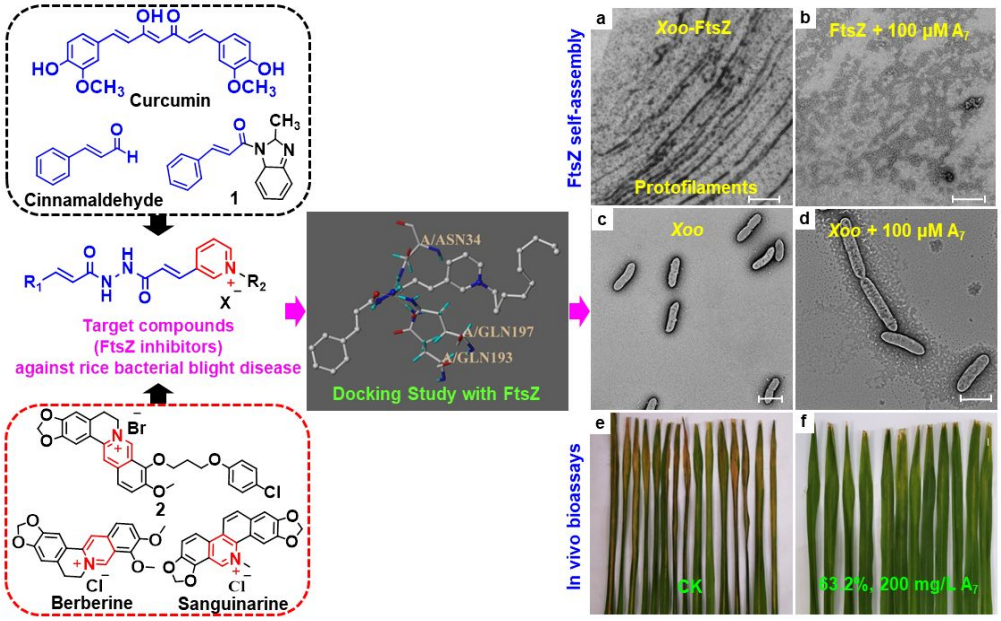

651